AD-A032 100 RAND CORP SANTA MONICA CALIF F/G 20/4
THREE-DIMENSIONAL FLOW SIMULATION IN ESTUARIES,(U)
JUN 75 J J LEENDERTSE, S LIU
UNCLASSIFIED P-5452 NL

1 OF 1
ADA032100

END

DATE
FILMED
1 -77

(2)

B.S.

THREE-DIMENSIONAL FLOW SIMULATION IN ESTUARIES

Jan J. Leendertse and Shiao-Kung Liu

June 1975

P-5452

The Rand Corporation
Santa Monica, California 90406

THREE-DIMENSIONAL FLOW SIMULATION IN ESTUARIES

Jan J. Leendertse and Shiao-Kung Liu
The Rand Corporation
Santa Monica, California 90406 U.S.A.

Jun 75 16 p.

SUMMARY

The model described in this paper is based upon numerical integration of the flow equations which simulate the water movements caused by tides, wind and pressure differences and upon numerical integration of the advective diffusion equation representing the movements of salt and temperature. The model neglects vertical accelerations, but not vertical velocities, and includes an approximation for the subgridscale effects by introduction of mass and momentum exchange coefficients. These coefficients are dependent upon the Richardson number and vertical velocity gradients. The computation method is tested on an estuary and the results of the simulations are presented in graph form.

P-5452

NOMENCLATURE

A_x, A_y = horizontal momentum dispersion coefficients
b = bottom layer
C = Chezy's coefficient
C^* = wind stress coefficient
D_x, D_y = horizontal mass-heat diffusion coefficients
f = Coriolis parameter
g = gravitational acceleration
$h(i,j,k)$ = layer thickness
i,j = horizontal grid index
k = vertical grid index
l = a layer index
m = a coefficient related to the vertical mass and heat diffusion coefficient
n = time level
p = pressure
r = a coefficient related to the vertical momentum diffusion coefficient
s = salinity
T = temperature
u,v,w = respective components of velocity
w_a = wind speed
x,y,z = Cartesian coordinates, positive eastward, northward and upward, respectively
δ = difference operation
ζ = water surface elevation with respect to the reference level, e.g., mean sea level
κ = vertical mass diffusion coefficient
κ' = vertical thermal diffusion coefficient
λ = a parameter related to the equation of state
ν = vertical momentum diffusion coefficient under nonisotropic vertical density gradient
ν_o = vertical momentum diffusion coefficient under neutrally stable density gradient (homogeneous)
ρ = density
$\bar{\rho}$ = reference density, a constant
ρ' = departure from $\bar{\rho}$ depending on salinity and temperature
τ = shear stresses
ϕ = wind direction

INTRODUCTION

In many estuaries, three-dimensional flows occur. The fresh river water often mixes only partially with denser sea water, and the salinity can change considerably over the depth. The currents induced by the density differences are superimposed upon the currents caused by tides and wind, causing very complicated current patterns.

The model described in this paper can effectively simulate these flow conditions by making the assumption that the vertical accelerations of the fluid are small. This assumption is generally justified. Neglecting the vertical accelerations but not the vertical velocities makes a mathematical formulation possible which permits a direct numerical integration of the equations representing the fluid flow.

The continuous fluid properties during simulation are expressed at discrete points, by which approach certain approximations are made; the approximations, however, are chosen in a manner that makes certain basic physical laws of the fluid still applicable. For example, no water disappears from the water body by the numerical procedures; also, energy in the horizontal motions is conserved, disregarding the losses by the representations for turbulent energy dissipation and the inputs by wind.

DYNAMIC EQUATIONS FOR TURBULENT ESTUARINE FLOW

The equations of horizontal motion for an incompressible internally source-free fluid on a rotating earth in Cartesian coordinates with the z axes positive upward are

$$\frac{\partial u}{\partial t} + \frac{\partial (uu)}{\partial x} + \frac{\partial (uv)}{\partial y} + \frac{\partial (uw)}{\partial z} - fv + \frac{1}{\rho}\frac{\partial p}{\partial x} - \frac{1}{\rho}\left(\frac{\partial \tau_{xx}}{\partial x} + \frac{\partial \tau_{xy}}{\partial y} + \frac{\partial \tau_{xz}}{\partial z}\right) = 0 \qquad (1)$$

$$\frac{\partial v}{\partial t} + \frac{\partial (vu)}{\partial x} + \frac{\partial (vv)}{\partial y} + \frac{\partial (vw)}{\partial z} + fu + \frac{1}{\rho}\frac{\partial p}{\partial y} - \frac{1}{\rho}\left(\frac{\partial \tau_{yx}}{\partial x} + \frac{\partial \tau_{yy}}{\partial y} + \frac{\partial \tau_{yz}}{\partial z}\right) = 0 \qquad (2)$$

If the vertical acceleration and advection are neglected, the equation of motion in the vertical direction becomes the hydrostatic equation

$$\frac{\partial p}{\partial z} + \rho g = 0 \qquad (3)$$

The equation of continuity is

$$\frac{\partial u}{\partial x} + \frac{\partial v}{\partial y} + \frac{\partial w}{\partial z} = 0 \qquad (4)$$

The equations of salt and heat balance are

$$\frac{\partial s}{\partial t} + \frac{\partial (us)}{\partial x} + \frac{\partial (vs)}{\partial y} + \frac{\partial (ws)}{\partial z} - \frac{\partial (D_x \frac{\partial s}{\partial x})}{\partial x} - \frac{\partial (D_y \frac{\partial s}{\partial y})}{\partial y} - \frac{\partial (\kappa \frac{\partial s}{\partial z})}{\partial z} = 0 \qquad (5)$$

$$\frac{\partial T}{\partial t} + \frac{\partial (uT)}{\partial x} + \frac{\partial (vT)}{\partial y} + \frac{\partial (wT)}{\partial z} - \frac{\partial (D_x \frac{\partial T}{\partial x})}{\partial x} - \frac{\partial (D_y \frac{\partial T}{\partial y})}{\partial y} - \frac{\partial (\kappa' \frac{\partial T}{\partial z})}{\partial z} = 0 \qquad (6)$$

and the equation of state

$$\rho = \bar{\rho} + \rho'(s,T) \qquad (7)$$

The representation of the estuarine system by Eqs. (1-7) includes no internal sources. In the equation for heat balance (Eq. (6)) we used the same diffusion coefficient as in the equation for the salt balance (Eq. (5)), which means that we neglected the heat fluxes by conduction and that only the fluxes by the turbulent fluid are considered.

The model described in this paper uses a grid system with equidistant points in the horizontal direction. In the vertical direction, however, the possibility of having an unequal grid distance was introduced, since vertical gradients which often occur in the estuaries can then be represented in detail without using a large number of grid points in the vertical.

In formulating the model, we introduce the concept of the layer. This is a geometrical concept only, and should not be confused with layers in stratified flow. The layers are determined by the introduction of a set of horizontal planes intersecting the body of the fluid. The thicknesses of the different layers are not necessarily the same for all layers.

The top layer, bounded by the free surface, has a time-variable height. In the formulation of the model the other layers may be intersected by the bottom and have a height which is dependent on the bathymetry. Figure 1 illustrates the grid system and the layers of the model. However, in our experiments we did not vary the bottom layer.

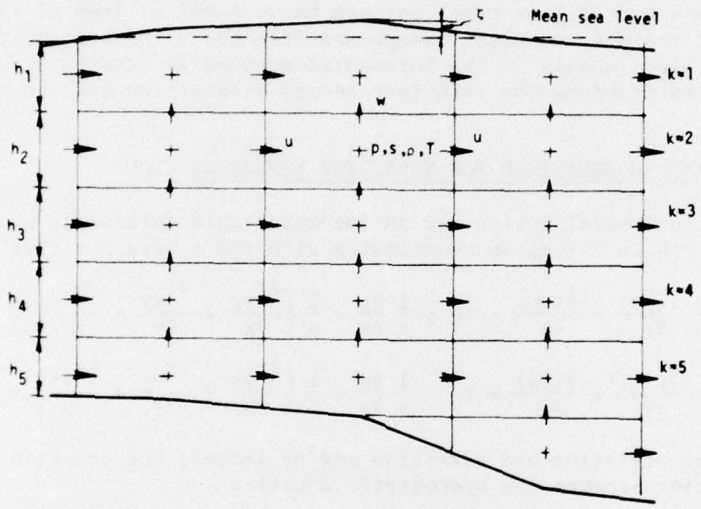

Fig. 1--Location of variables on the vertical grid

In the computational model, the origin of the coordinates is taken at the mean sea level, whereas the water surface $z = \zeta(x,y,t)$ is the upper boundary of the system.

The description of the finite-difference equations from the differential equations was accomplished in two steps: first, the equations for the layers were derived by vertically integrating the variables over the layer thickness, and subsequently finite-difference approximations for the layer equations were developed. We have shown in Refs. 1 and 2 that the vertically integrated momentum equations can be written for each layer (Fig. 1) using u and v for layer average values of the velocity components.

$$\frac{\partial(hu)}{\partial t} + \frac{\partial(huu)}{\partial x} + \frac{\partial(hvu)}{\partial y} + (uw)_{k-\frac{1}{2}} - (uw)_{k+\frac{1}{2}} - fhv + \frac{h}{\rho}\frac{\partial p}{\partial x} + \left(\frac{1}{\rho}\tau^{xz}\right)_{k+\frac{1}{2}} - \left(\frac{1}{\rho}\tau^{xz}\right)_{k-\frac{1}{2}} - \frac{1}{\rho}\frac{\partial(hA_x\frac{\partial u}{\partial x})}{\partial x} - \frac{1}{\rho}\frac{\partial(hA_y\frac{\partial u}{\partial y})}{\partial y} = 0 \qquad (8)$$

$$\frac{\partial(hv)}{\partial t} + \frac{\partial(hvu)}{\partial x} + \frac{\partial(hvv)}{\partial y} + (vw)_{k-\frac{1}{2}} - (vw)_{k+\frac{1}{2}} + fhu + \frac{h}{\rho}\frac{\partial p}{\partial y} + \left(\frac{1}{\rho}\tau^{yz}\right)_{k+\frac{1}{2}} - \left(\frac{1}{\rho}\tau^{yz}\right)_{k-\frac{1}{2}} - \frac{1}{\rho}\frac{\partial(hA_x\frac{\partial v}{\partial x})}{\partial x} - \frac{1}{\rho}\frac{\partial(hA_y\frac{\partial v}{\partial y})}{\partial y} = 0 \qquad (9)$$

The formulation of these equations of motion differs from the more classical representations presented, for example, by Bowden (Ref. 3) and Pritchard (Ref. 4), in that our equations are conceptionally well traceable and contain the derivatives of products of variables rather than products of variables and derivatives. Except for the density and the spatial and time derivative, no dividers are present, i.e., when finite-difference approximations of these equations are used, the number of divisions is limited.

The heat and salt balance equations can be presented in the same form for each layer k:

$$\frac{\partial(hs)}{\partial t} + \frac{\partial(hus)}{\partial x} + \frac{\partial(hvs)}{\partial y} + (ws)_{k-\frac{1}{2}} - (ws)_{k+\frac{1}{2}} - \frac{\partial(hD_x \frac{\partial s}{\partial x})}{\partial x} - \frac{\partial(hD_y \frac{\partial s}{\partial y})}{\partial y} + (\kappa \frac{\partial s}{\partial z})_{k+\frac{1}{2}} - (\kappa \frac{\partial s}{\partial z})_{k-\frac{1}{2}} = 0 \tag{10}$$

$$\frac{\partial(hT)}{\partial t} + \frac{\partial(huT)}{\partial x} + \frac{\partial(hvT)}{\partial y} + (wT)_{k-\frac{1}{2}} - (wT)_{k+\frac{1}{2}} - \frac{\partial(hD_x \frac{\partial T}{\partial x})}{\partial x} - \frac{\partial(hD_y \frac{\partial T}{\partial y})}{\partial y} + (\kappa' \frac{\partial T}{\partial z})_{k+\frac{1}{2}} - (\kappa' \frac{\partial T}{\partial z})_{k-\frac{1}{2}} = 0 \tag{11}$$

From the equation of continuity we derived for the time derivative of the water surface

$$\frac{\partial \zeta}{\partial t} + \sum_{\ell=1}^{\ell=b} \left| \frac{\partial(hu)}{\partial x} + \frac{\partial(hv)}{\partial y} \right|_{\ell} = 0 \tag{12}$$

and for the vertical velocity at the interface between layer k and k - 1

$$w_{k-\frac{1}{2}} = - \sum_{\ell=k}^{\ell=b} \left| \frac{\partial(hu)}{\partial x} + \frac{\partial(hv)}{\partial y} \right|_{\ell} \tag{13}$$

The horizontal pressure gradient in the top layer was approximated by

$$\left.\begin{aligned} \frac{\partial p_1}{\partial x} &= g\rho_1 \frac{\partial \zeta}{\partial x} + \tfrac{1}{2} g h_1 \frac{\partial \rho_1}{\partial x} \qquad (14) \\ \frac{\partial p_1}{\partial y} &= g\rho_1 \frac{\partial \zeta}{\partial y} + \tfrac{1}{2} g h_1 \frac{\partial \rho_1}{\partial y} \qquad (15) \end{aligned}\right\} k = 1$$

where ρ_1 = layer average density of the top layer. The pressure gradient for the other layers is

$$\left.\begin{aligned} \frac{\partial p_k}{\partial x} &= \frac{\partial p_{k-1}}{\partial x} + g h_{k-\frac{1}{2}} \frac{\partial \rho_{k-\frac{1}{2}}}{\partial x} \qquad (16) \\ \frac{\partial p_k}{\partial y} &= \frac{\partial p_{k-1}}{\partial y} + g h_{k-\frac{1}{2}} \frac{\partial \rho_{k-\frac{1}{2}}}{\partial y} \qquad (17) \end{aligned}\right\} k = 2, 3 \ldots b$$

where $\rho_{k-\frac{1}{2}} = \frac{1}{2}(\rho_{k-1} + \rho_k)$

ρ_k = layer average density of layer k.

FINITE-DIFFERENCE FORMULATION AND APPROXIMATION

A space-staggered grid (Fig. 2) was selected for the finite-difference approximation of Eqs. (8) through (17). The pressure p, salinity s, and temperature T are computed at integer values of i, j, and k. The velocity components u are computed at half-integer values of i and integer values of j and k, and the velocity components v are computed at integer values of i and k and half-integer values of j. The vertical velocity components w are computed at integer values of i and j, and half-integer values of k (see Fig. 3). The water surface elevation ζ is expressed only on a two-dimensional horizontal grid and has integer values of i and j.

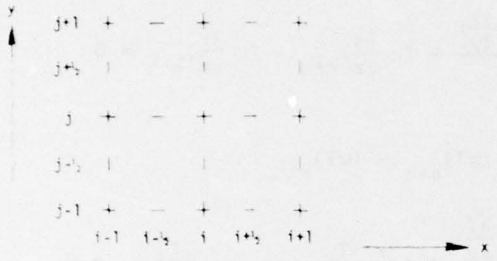

Fig. 2--The location of u (—), v (|), and other parameters (+) in the space-staggered grid

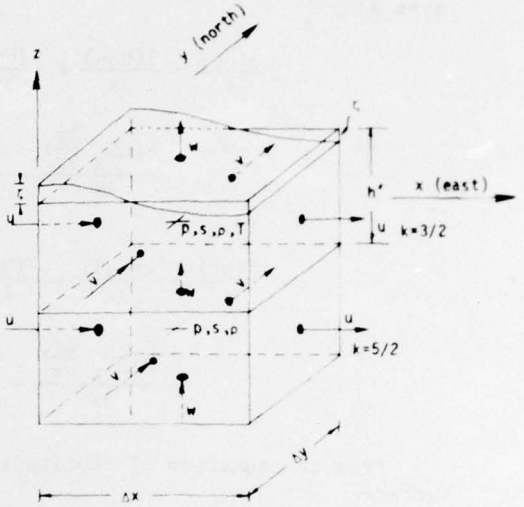

Fig. 3--Relative position of the variables in the model

A compact notation was introduced which not only describes the finite-difference approximation accurately, but also gives this approximation the same appearance as the differential equations. The position of the variables in the horizontal grid is indicated by indices i,j, indicating a position $i\Delta x$ and $j\Delta y$ from the origin of the coordinates, with i,j = 0, ±½, ±1, ±3/2.

The vertical position is determined as to its location in the center of the layer numbered from the top with integer k = 1, 2, 3 ... or at the horizontal interfaces with half-integer values k = 1/2, 3/2, 5/2 ...

Time is determined by the number of time steps ($n\Delta t$) from the reference time, with n an integer value.

The following sum and difference notations are adopted:

$$\overline{F}^{x} = \tfrac{1}{2}\left\{F[(i + \tfrac{1}{2})\,\Delta x, j\Delta y, k\Delta z, n\Delta t] + F[(i - \tfrac{1}{2})\,\Delta x, j\Delta y, k\Delta z, n\Delta t]\right\} \tag{18}$$

$$\delta_x F = \frac{1}{\Delta x}\left\{F[(i + \tfrac{1}{2})\,\Delta x, j\Delta y, k\Delta z, n\Delta t] - F[(i - \tfrac{1}{2})\,\Delta x, j\Delta y, k\Delta z, n\Delta t]\right\} \tag{19}$$

These are shown only for x, but are also used for y, z, and t.

The special notation used for shifted time levels is

$$F_{+} = F[i\Delta x, j\Delta y, k\Delta z, (n + 1)\Delta t] \tag{20}$$

$$F_{-} = F[i\Delta x, j\Delta y, k\Delta z, (n - 1)\Delta t] \tag{21}$$

With these space-time sum-differencing operators, the finite-difference approximations of Eqs. (8) through (17), for the level k with layer-average values, take the following form:

$$\overline{\delta_t \zeta}^t = - \sum_k \left| \delta_x(\overline{h}^x u) + \delta_y(\overline{h}^y v) \right| \qquad \text{at } i, j, n \tag{22}$$

$$\begin{aligned}\overline{\delta_t(\overline{h}^x u)}^t = &- \delta_x(\overline{\overline{h}^x u}^x \overline{u}^x) - \delta_y(\overline{\overline{h}^y v}^x \overline{u}^y) - \overline{h}^x \delta_z(\overline{u}^z \overline{w}^x) \\ &+ f\overline{h}^x \overline{v}^{xy} - \frac{1}{\overline{\rho}^x} \overline{h}^x \delta_x p - \frac{1}{\overline{\rho}^x}\left[\left(\tau^{xz}_-\right)_{k+\frac{1}{2}} + \left(\tau^{xz}_-\right)_{k-\frac{1}{2}}\right] \\ &+ \frac{1}{\overline{\rho}^x}\left[\delta_x\left|\overline{\overline{h}^x A_x}^x \delta_x u\right|_- + \delta_y\left|\overline{\overline{h}^x A_y}^y \delta_y u\right|_-\right] \qquad \text{at } i + \tfrac{1}{2}, j, k, n\end{aligned} \tag{23}$$

$$\begin{aligned}\overline{\delta_t(\overline{h}^y v)}^t = &- \delta_x(\overline{\overline{h}^x u}^y \overline{v}^x) - \delta_y(\overline{\overline{h}^y v}^y \overline{v}^y) - \overline{h}^y \delta_z(\overline{v}^z \overline{w}^y) \\ &- f\overline{h}^y \overline{u}^{xy} - \frac{1}{\overline{\rho}^y} \overline{h}^y \delta_y p - \frac{1}{\overline{\rho}^y}\left[\left(\tau^{yz}_-\right)_{k+\frac{1}{2}} + \left(\tau^{yz}_-\right)_{k-\frac{1}{2}}\right] \\ &+ \frac{1}{\overline{\rho}^y}\left[\delta_x\left|\overline{\overline{h}^y A_x}^x \delta_x v\right|_- + \delta_y\left|\overline{\overline{h}^y A_y}^y \delta_y v\right|_-\right] \qquad \text{at } i, j + \tfrac{1}{2}, k, n\end{aligned} \tag{24}$$

$$\begin{aligned}\overline{\delta_t(hs)}^t = &- \delta_x(\overline{h}^x u \overline{s}^x) - \delta_y(\overline{h}^y v \overline{s}^y) - h\delta_z(w\overline{s}^z) \\ &+ \delta_x\left|\overline{h}^x D_x \delta_x s\right|_- + \delta_y\left|\overline{h}^y D_y \delta_y s\right|_- - \left(\kappa \delta_z s_-\right)_{k+\frac{1}{2}} + \left(\kappa \delta_z s_-\right)_{k-\frac{1}{2}} \\ &\qquad \text{at } i, j, k, n\end{aligned} \tag{25}$$

$$\begin{aligned}\overline{\delta_t(hT)}^t = &- \delta_x(\overline{h}^x u \overline{T}^x) - \delta_y(\overline{h}^y v \overline{T}^y) - h\delta_z(w\overline{T}^z) \\ &+ \delta_x\left|\overline{h}^x D_h \delta_x T\right|_- + \delta_y\left|\overline{h}^y D_h \delta_y T\right|_- - \left(\kappa' \delta_z T_-\right)_{k+\frac{1}{2}} + \left(\kappa' \delta_z T_-\right)_{k-\frac{1}{2}} \\ &\qquad \text{at } i, j, k, n\end{aligned} \tag{26}$$

The density is computed using s(i,j,k,n) and T(i,j,k,n) according to the equation of state:

$$\begin{aligned}\rho = &\left[5890 + 38T - 0.375T^2 + 3s\right] \Big/ \left[(1779.5 + 11.25T - 0.0745T^2)\right. \\ &\left. - (3.8 + 0.01T)s + 0.698(5890 + 38T - 0.375T^2 + 3s)\right] \qquad \text{at } i, j, k, n + 1\end{aligned} \tag{27}$$

A graphical representation of the density as a function of temperature for water with different salinity is shown in Fig. 4. The finite-difference equation used to compute the vertical velocities is

$$\delta_z w = - \delta_x(\overline{h}^x u) - \delta_y(\overline{h}^y v) \qquad \text{at } i, j, k, n + 1 \tag{28}$$

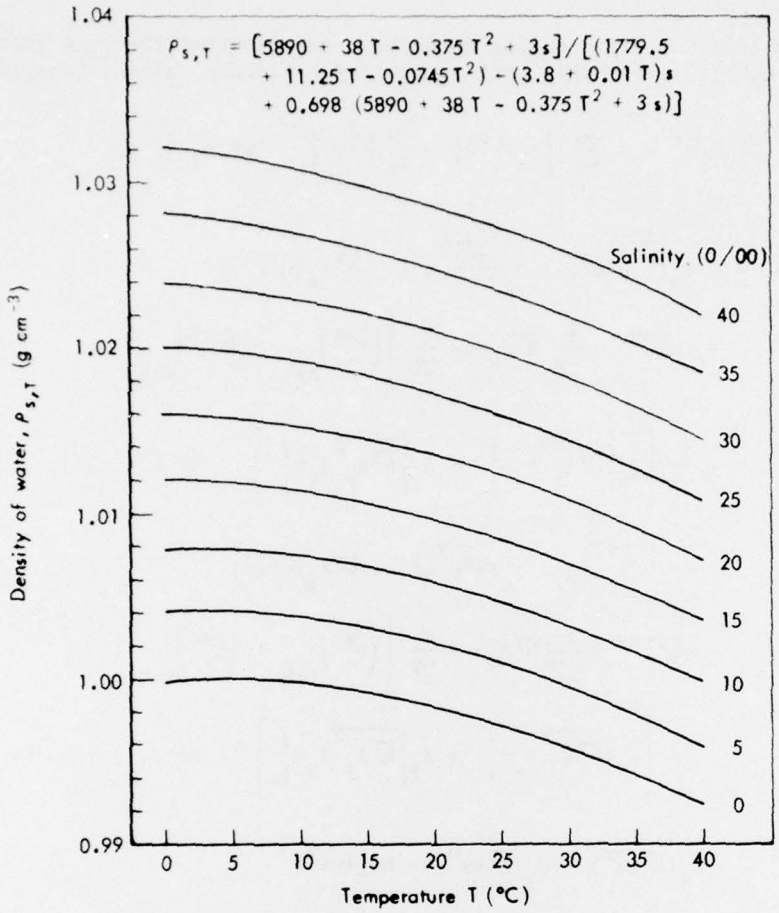

Fig. 4--Equation of state and graphical representations of several selected ranges of s and T values

This equation is used for the bottom layer first and then for the layer above, etc. The horizontal pressure gradients are computed first in the top layer:

$$\delta_x p = g(\widetilde{\rho}^x \delta_x \zeta) + \tfrac{1}{2}\,\overline{h}^x \delta_x \rho \qquad \text{at } i + \tfrac{1}{2},\ j,\ 1,\ n + 1 \tag{29}$$

$$\delta_y p = g(\widetilde{\rho}^y \delta_y \zeta) + \tfrac{1}{2}\,\overline{h}^y \delta_y \rho \qquad \text{at } i,\ j + \tfrac{1}{2},\ 1,\ n + 1 \tag{30}$$

Then the pressure gradients are computed with increasing k by use of

$$\delta_z(\delta_x p) = g\delta_x \overline{\rho}^z \qquad \text{at } i + \tfrac{1}{2},\ j,\ k + p,\ n + 1 \tag{31}$$

$$\delta_z(\delta_y p) = g\delta_y \overline{\rho}^z \qquad \text{at } i,\ j + p,\ k + \tfrac{1}{2},\ n + 1 \tag{32}$$

Once the horizontal pressure gradients are known, the water level and velocities can be computed again by the sequence of finite difference equations (22) through (32).

Special procedures are required for the computation of variables on or near the boundaries. The seaward boundary presents particular problems, as described in Ref. 2.

VERTICAL MASS AND MOMENTUM EXCHANGE COEFFICIENTS

In fluids with vertically stable or unstable density gradients, the model assesses the vertical momentum exchange, vertical mass-heat diffusion coefficients according to the following Richardson number related formulas (Ref. 2). For the vertical momentum exchange:

$$\left(\tau_{-}^{xz}\right)_{k+\frac{1}{2}} = \overline{\rho}^{xz}\left(\nu_o \exp\left\{-m\frac{g}{\overline{\rho}^{xz}}\frac{\delta_z(\overline{\rho}^{x})}{[\delta_z(u_{-})]^2}\right\} + \nu_1\left[\left(\delta_z u_{-}\right)^2 + \left(\delta_z \overline{v}^{xy}\right)^2\right]^{\frac{1}{2}}\right)\left(\delta_z u_{-}\right)$$

$$\text{at } i+\tfrac{1}{2}, j, k+\tfrac{1}{2}, n \qquad (33)$$

$$\left(\tau_{-}^{yz}\right)_{k+\frac{1}{2}} = \overline{\rho}^{yz}\left(\nu_o \exp\left\{-m\frac{g}{\overline{\rho}^{yz}}\frac{\delta_z(\overline{\rho}^{y})}{[\delta_z(v_{-})]^2}\right\} + \nu_1\left[\left(\delta_z \overline{u}^{xy}\right)^2 + \left(\delta_z v_{-}\right)^2\right]^{\frac{1}{2}}\right)\left(\delta_z v_{-}\right)$$

$$\text{at } i, j+\tfrac{1}{2}, k+\tfrac{1}{2}, n \qquad (34)$$

For the vertical diffusion-dispersion of salt and heat:

$$\left(\kappa\partial_z S_{-}\right)_{k+\frac{1}{2}} = \left\{\nu_o \exp\left[-\frac{rg}{\overline{\rho}^{z}}\frac{\delta_z\rho}{(\delta_z U)^2}\right] + \kappa_1\delta_z U\right\}\delta_z S_{-} \qquad \text{at } i,j,k+\tfrac{1}{2}n \qquad (35)$$

and

$$\left(\kappa'\delta_z T_{-}\right)_{k+\frac{1}{2}} = \left\{\nu_o \exp\left[-\frac{rg}{\overline{\rho}^{z}}\frac{\delta_z\rho}{(\partial_z U)^2}\right] + \kappa_1'\delta_z U\right\}\delta_z T_{-} \qquad \text{at } i,j,k+\tfrac{1}{2},n \qquad (36)$$

where

$$\delta_z U = \left\{\left(\delta_z \overline{u}^{x}\right)^2 + \left(\delta_z \overline{v}^{y}\right)^2\right\}^{\frac{1}{2}} \qquad (37)$$

where m,r = exponents, equal to 0.4 and 0.8, respectively, according to Mamayev (Ref. 5).

A quadratic expression was used for surface wind-induced stress and bottom current-induced drag.

$$\frac{1}{\overline{\rho}^{x}}\left(\tau_{-}^{xz}\right)_{k-\frac{1}{2}} = C^*\frac{\rho_a}{\overline{\rho}^{x}}w_a^2\sin\phi \qquad \text{at } i+\tfrac{1}{2}, j, 1, n \qquad (38)$$

$$\frac{1}{\overline{\rho}^{y}}\left(\tau_{-}^{yz}\right)_{k-\frac{1}{2}} = C^*\frac{\rho_a}{\overline{\rho}^{y}}w_a^2\cos\phi \qquad \text{at } i, j+\tfrac{1}{2}, 1, n \qquad (39)$$

$$\frac{1}{\overline{\rho}^{x}}\left(\tau_{-}^{xz}\right)_{k+\frac{1}{2}} = gu_{-}\left[u_{-}^2 + (\overline{v}_{-}^{xy})^2\right]^{\frac{1}{2}}\Big/\,(\overline{C}^{x})^2 \qquad \text{at } i+\tfrac{1}{2}, j, b, n \qquad (40)$$

$$\frac{1}{\overline{\rho}^{y}}\left(\tau_{-}^{yz}\right)_{k+\frac{1}{2}} = gv_{-}\left[(\overline{u}_{-}^{xy})^2 + v_{-}^2\right]^{\frac{1}{2}}\Big/\,(\overline{C}^{y})^2 \qquad \text{at } i, j+\tfrac{1}{2}, b, n \qquad (41)$$

No thermal or salinity fluxes at the bottom are introduced, and the exchanges at the bottom can be set to zero.

NUMERICAL EXPERIMENTS

To illustrate the model's operation, we present two sample cases. The first one involves the simulation of three-dimensional wind-driven circulation in a rectangular basin. This basin was 3400 m long, 1400 m wide, and 7 m deep. This rectangular basin was then schematized into a grid structure of 17 × 7 × 7 with $\Delta x = \Delta y = 200$ m and $\Delta z = 1$ m. The water was at rest at the beginning (t = 0). A diagonal wind stress of 10

dynes/cm^2 (approximately equivalent to 40 mph) was applied, and the simulation was carried out to 2000 timesteps with Δt = 5 sec. Figure 5 shows the vertical sections through the longest axis of the basin in a sequence (a,b,c and d) representing the system's transient response under wind stress. Each graph, with the simulation time step indicated at the lower left corner, shows the sequential development of the wind-induced circulation pattern in the x-z direction. In these graphs the vertical scale has been enlarged 200 times, and also the vertical velocity components (i.e., w) are multiplied by 200 before the computation of the x-z velocity vectors at each grid point.

In the beginning only a surface current is set up by the wind stress (Fig. 5a). Figure 5b shows the penetration of surface current to the deeper layers through the viscosity and vertical advection effects, and vertical velocity components at two ends of the basin. Figures 5c and 5d show the generation of two large vertical eddies, while the surface current gradually penetrates from the surface layer through the bottom. Figure 6a shows the two elongated eddies finally breaking up and merging into one large basin-sized eddy forming a layered flow structure. At the 75th time step (Figs. 6a through 6h), a quasi-steady state circulation is almost established. The effect of bottom friction becomes more pronounced as the undercurrent reaches its maturity. The current delimitation plane between the surface current and the return current is moved upward due to the bottom current's retardation.

Figure 7 shows the time histories of the multilayered current at the center section of the basin for the entire simulation period. The duration of the simulation is selected approximately equal to ten times the basin oscillation period of the basin (equal to approximately 164 time steps). In the first few hundred steps the current field becomes established and the basin-wide circulation cell is generated. At the beginning of the computation, wind stress suddenly applies energy to the system. Consequently, the basin also starts to oscillate and the velocities belonging to this oscillation are superimposed upon those of the wind-driven circulation. The mean velocities at the top and bottom layer are shown as dashed lines. At step 500 the wind stress is removed and the circulation decays. The oscillation of the basin, however, persists.

The Chesapeake Bay system in the eastern part of the United States was also selected for a numerical experiment. The hydrodynamic behavior of Chesapeake Bay is characterized by its circulatory responses under four major driving and modifying forces, namely, tide, wind, river inflow, and Coriolis forces. The geometry of Chesapeake Bay is schematized into a computational grid network of 40 × 100 × 6, with $\Delta x = \Delta y$ = 3000 m. The thickness of the top five layers is 4 m each, with the last layer being 8 m.

Figure 8 is a typical simulation output map showing the horizontal circulatory pattern for the top layer at time step 4000, with Δt = 60 sec (i.e., 66.7 hr). The ratio between the length of a velocity vector and a grid size for this particular case is 30 cm/sec. The heavy outline denotes the water's edge at the lower low water, whereas a thin dash line delineates the 20-ft-bottom contour line. On this map, the horizontal velocity field is represented by the velocity isolines. At this point in time, the tide level at the open boundary is near its low slack water (see input tide at the lower right corner).

In the upper bay water flows generally to the north. The vertical circulation pattern at a few selected sections can be seen from the vertical current profiles in the upper right corner of Fig. 8.

CONCLUSIONS

The three-dimensional flows in estuaries with nonisotropic density distributions can effectively be computed according to the finite difference method described in this paper. The model required coefficients used in describing the small-scale mass and momentum exchanges. These coefficients must be found experimentally from field data.

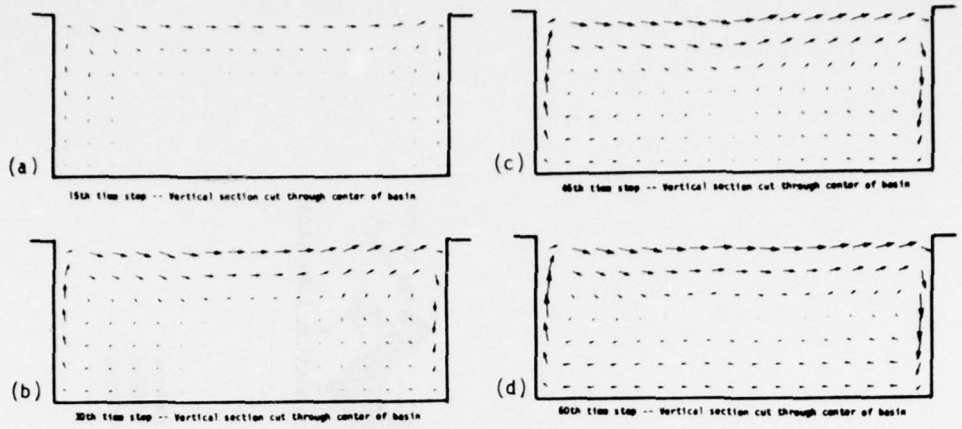

Fig. 5--The transient response in a vertical cross-section of a rectangular basin under a diagonal wind stress

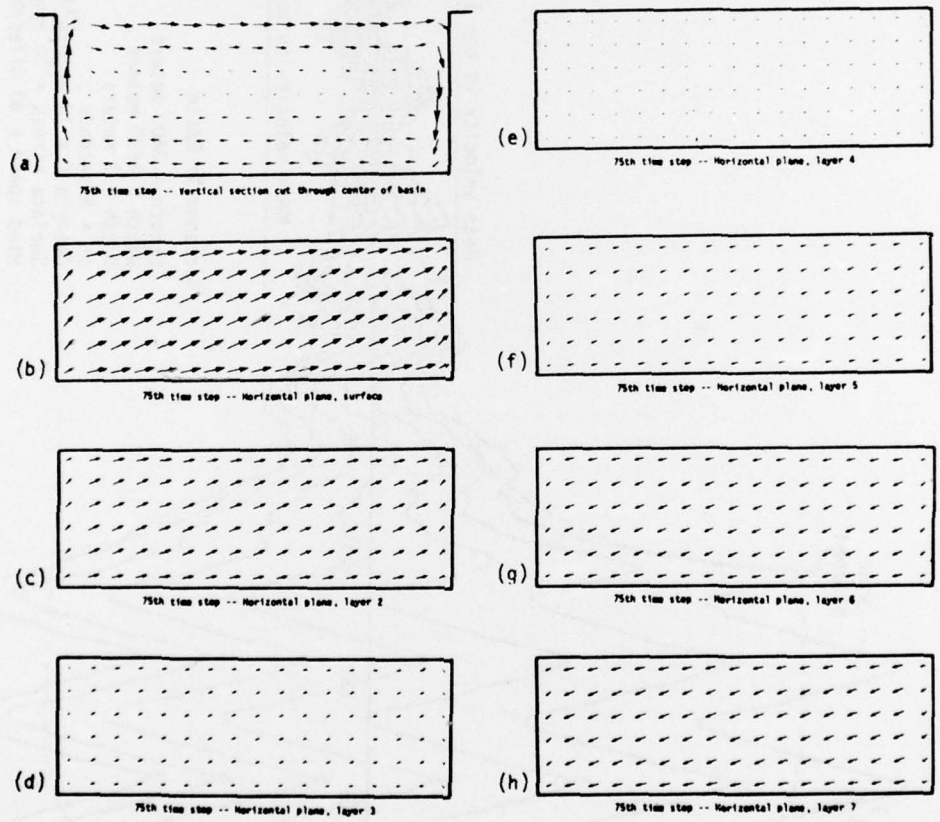

Fig. 6--Velocity components in a cross-section and in seven horizontal layers of a wind-driven rectangular basin at the 75th time step of the computation

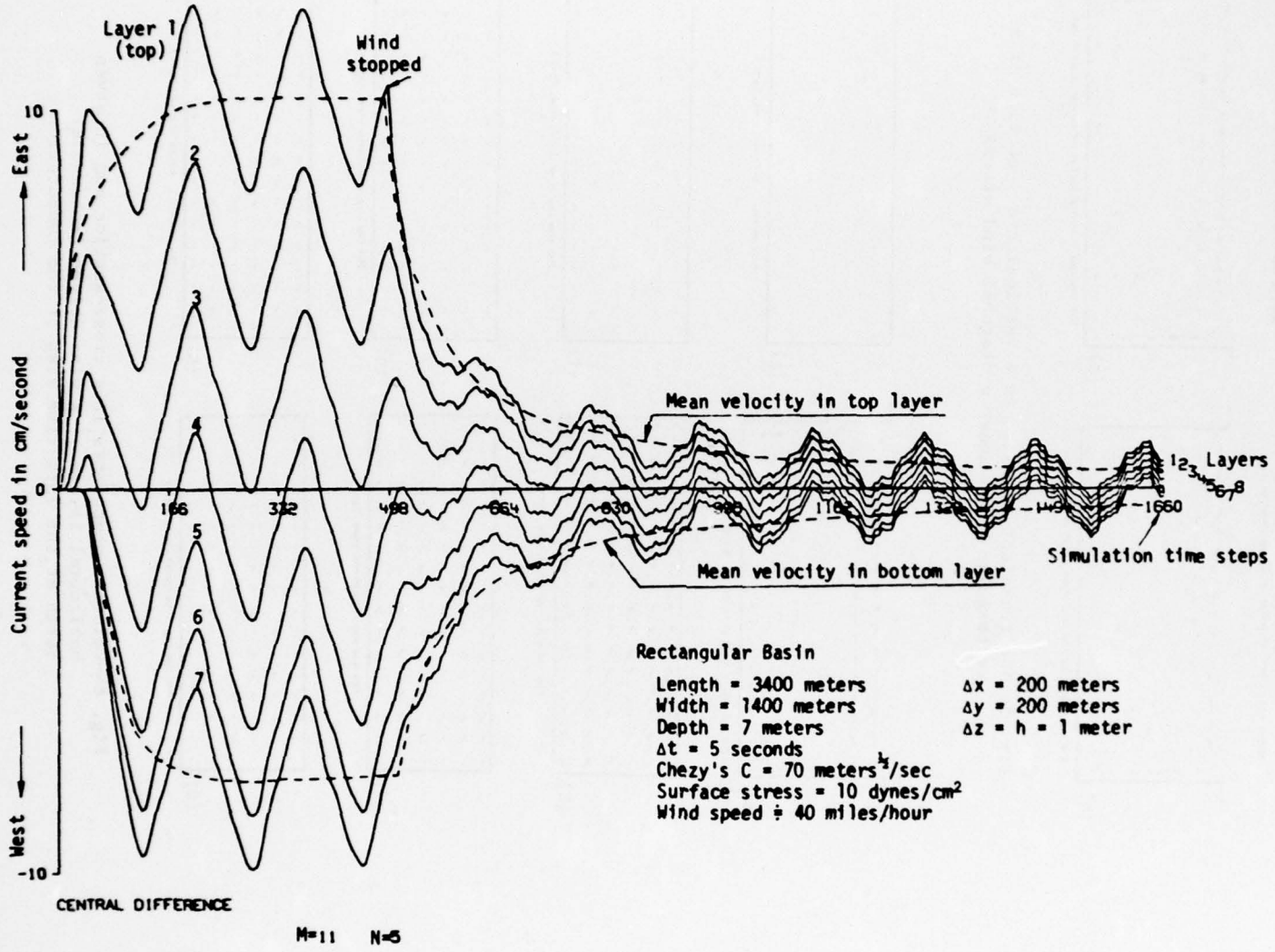

Fig. 7--Time history of the multi-layer wind-driven current speed at the center of the basin

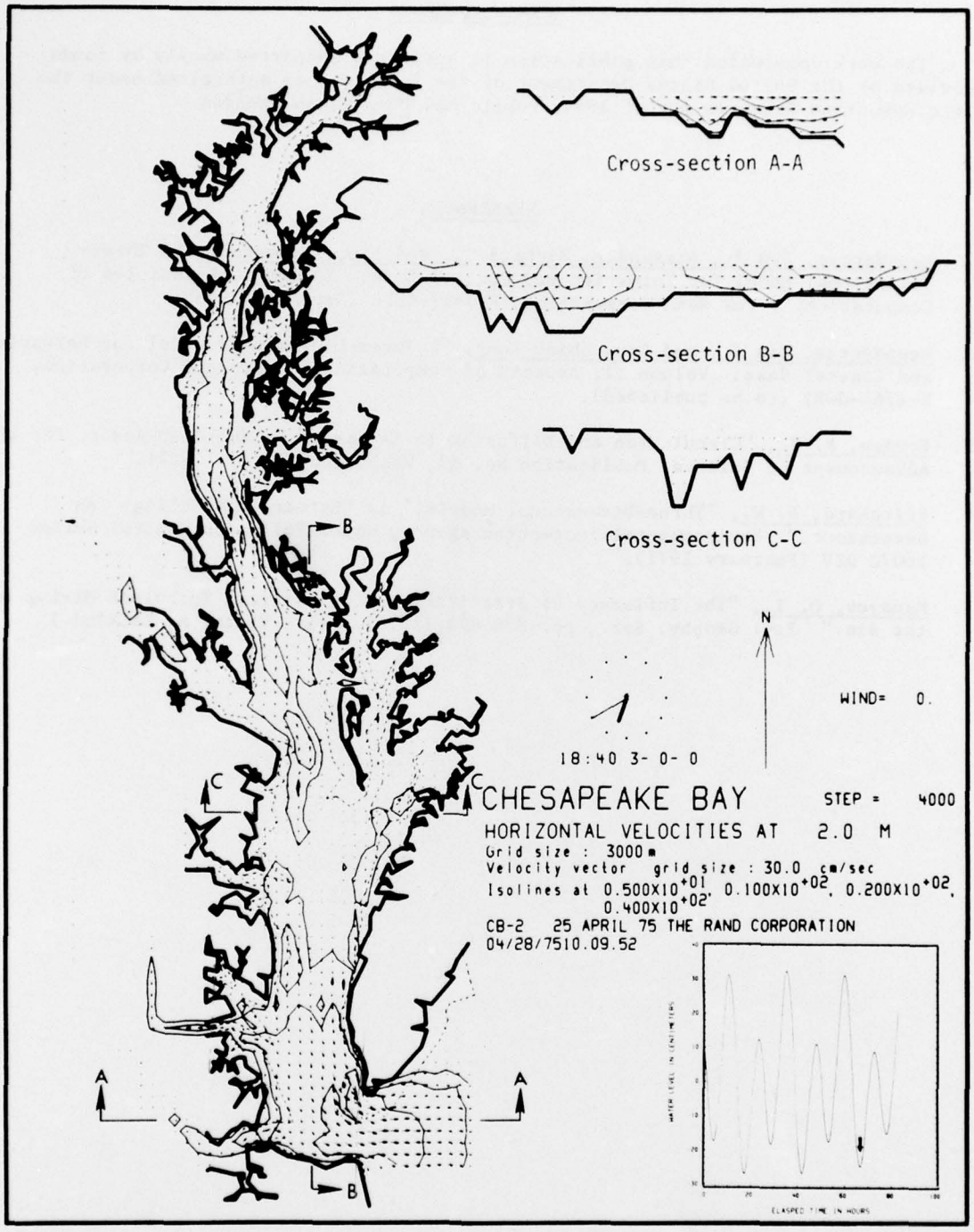

Fig. 8--A typical current map showing the spatial distribution of the velocity field at 2.0 m and the vertical circulation through three selected cross-sections of Chesapeake Bay, U.S.A.

ACKNOWLEDGMENTS

The work upon which this publication is based was supported wholly by funds provided by the United States Department of the Interior, as authorized under the Water Resources Research Act of 1964, Public Law 88-379, as amended.

REFERENCES

1. Leendertse, Jan J., Alexander, Richard C., and Liu, Shiao-Kung, "A Three-Dimensional Model for Estuaries and Coastal Seas: Volume I, Principles of Computation." The Rand Corporation, R-1417-OWRR (December 1973).

2. Leendertse, Jan J., and Liu, Shiao-Kung, "A Three-Dimensional Model for Estuaries and Coastal Seas: Volume II, Aspects of Computation." The Rand Corporation, R-1764-OWRT (to be published).

3. Bowden, K. F., "Circulation and Diffusion in Estuaries." American Assoc. for the Advancement of Science, Publication No. 83, Washington, D.C. (1967).

4. Pritchard, D. W., 'Three-Dimensional Models,' in "Estuarine Modeling: An Assessment." Environmental Protection Agency, Water Pollution Control Series 16070 DZV (February 1971).

5. Mamayev, O. I., "The Influence of Stratification on Vertical Turbulent Mixing in the Sea." Izv. Geophy. Ser., pp. 870-875 (1958). (Tr. Victor A. Salkind.)